Chapter 4
Woody Biomass Change Monitoring in Temperate Montane Forests by Airborne LiDAR Analysis

Yoshio Awaya

Abstract Airborne laser scanners by light detection and ranging (LiDAR) measure the elevation of ground objects, and canopy height (DCHM) can be estimated as the difference between the canopy surface and ground elevation. A forest area was selected in the east of Takayama city (Gifu Prefecture, Japan) in the cool temperate forest zone. Airborne LiDAR observation was executed in 2005 and 2011. Total dry woody biomass (TDB) was mapped using the two LiDAR data using statistical biomass estimation models, one for evergreen coniferous forests and the other for deciduous broadleaved forests using DCHMs. Changes in TDB were mapped, and man-made evergreen coniferous forests surrounding a village in the west showed greatest TDB and growth in the study area due to human forestry activity. On the other hand, forests in the east were young with less TDB and growth. Hence, forests in the east were younger, and TDB and growth were less, than those in the west. Deciduous broadleaved forests, which were used as fuel woods until the 1960s, generally had smaller TDB and growth. Human forestry activity resulted in TDB and growth differences, and TDB maps showed impacts of the forestry activity in this area.

Keywords Total dry biomass (TDB) · Biomass growth · Airborne LiDAR · Cool temperate forest · Forestry activity

4.1 Introduction

A forest ecosystem provides various ecosystem services, including carbon stock and fixation, timber and fuel supply, water purification, and wildlife habitat. It is essential to identify the forest distribution including forest type, height, and biomass to understand the contribution of a forest to the human community through its ecosystem services. For example, different (e.g. by species, height, density, and age) forest

Y. Awaya (✉)
River Basin Research Center, Gifu University, Gifu, Japan
e-mail: awaya@green.gifu-u.ac.jp

F. Li et al. (eds.), *River Basin Environment: Evaluation, Management and Conservation*, https://doi.org/10.1007/978-981-19-4070-5_4

types support different animals, and geographical forest information is probably necessary and important for animal conservation.

Forest resource information is mandatory for forestry. Stock volume information (both amount and distribution) is important for timber production, and dry biomass information is necessary when calculating the woody fuel supply. Since timber is a renewable resource, it is important to use biomass wisely in order to reduce carbon emissions. Recently, biomass and carbon fixation information from each forest is required for global warming mitigation as well.

The concentration of atmospheric carbon dioxide (CO_2), one of the greenhouse gasses causing climate change, is increasing steadily. Moreover, global mean air temperature seems to have increased greatly since the 1910s in conjunction with the increasing greenhouse gas concentration (Houghton et al. 2001). Internationally there is much interest in the estimation of carbon storage and evaluation of carbon balance in terrestrial ecosystems in order to understand the potential value of ecosystems for carbon reduction.

Net primary productivity (NPP), which is the amount of carbon absorbed by vegetation, may increase under increasing global air temperature in ecosystems where plants can extend the growing period. On the other hand, decreased precipitation may cause NPP reduction in ecosystems due to water stress (Houghton et al. 2001). Estimation of NPP is essential for evaluating the carbon balance, and for understanding the effects of climate change on vegetation.

Biomass is an important variable for forestry as a resource as well as a CO_2 source for carbon balance studies. The biomass and carbon stocks in forests are important indicators of their productive capacity, energy potential, and capacity to sequester carbon (FAO 2016). Biomass is a pool of atmospheric carbon fixed by plants and ranges widely based on tree size in large areas. The difference between biomass and litter falls during a period (usually a year) is the NPP. On the other hand, it is well known that forest disturbances in the tropics release carbon to the atmosphere as CO_2. In addition, tree plantations and silvicultural treatments in some countries such as China result in significant tree growth and support carbon fixation from the atmosphere to trees (FAO 2016). Therefore understanding forest change as the potential carbon sink in a large area is essential for understanding carbon balance on a regional, national, continental, or global scale. However, precise assessment of forest biomass distribution by field survey is a difficult task when the area is large.

Remote sensing provides information concerning landcover by detecting signals such as reflected solar energy from the land surface and analyzing characteristics of signals. For example, optical sensors provide multispectral surface information as digital images (pictures) of a certain mesh size between sub-meter and some kilometers. Optical sensors separate reflected solar energy into some different wavelengths, which is spectra. Obtained images cover areas from about 100 km^2 to 300,000 km^2 as wall-to-wall pixel data and are used for forestry applications.

Thus optical images can be used to estimate spatial coverage of forest information, such as forest types and biomass (Franklin 2001). Providing information in large areas is the greatest advantage of remote sensing, and this technology surpasses the field survey method. On the other hand, the greatest problem of optical sensors is

that they observe not only biophysical parameter directly but also the spectra (color) of trees. Therefore forest information such as biomass is evaluated indirectly (indirect estimation) by identifying any relationship between intensity of spectral reflectance and biophysical parameters such as biomass. Relationships between reflectance and biophysical parameters are not strong and change according to the images. Since observed reflectance values change according to different specifications of the sensors, observation conditions such as atmosphere, solar direction, and topographic shadow. Although removing influence or 'noise' using these factors is mandatory, removing noise is a very hard task. As a result, it is difficult to derive consistent and accurate estimation of biophysical parameters because of the indirect estimation affected by numerous noise sources.

Although optical remote sensing has been used to estimate forest biomass distribution (Peng et al. 2019; Spanner et al. 1990; Peterson et al. 1987), it is very difficult to derive accurate and consistent estimation from optical images due to not only atmospheric and topographic effects but also seasonal changes of tree spectra. Reflectance is saturated in stands with high biomass and the estimation accuracy is low in dense forests with high biomass (Foody et al. 2003). Optical images have been also used for estimation of NPP distribution and for their inter-annual monitoring with environment information such as climate (e.g. air temperature and precipitation) (Awaya et al. 2004; Potter et al. 1993).

The normalized difference vegetation index (NDVI) is linear to the fraction of absorbed photosynthetically active radiation, and NDVI can be used to estimation the amount of solar energy which is used photosynthesis by plants. It is essential to achieve very accurate atmospheric correction, topographic correction, and reduction of effects of bidirectional reflectance distribution function (BRDF) of vegetation species-by-species for precise optical image processing to derive biophysical parameters including biomass and NPP. However accurate high resolution atmospheric information maps for atmospheric correction are not available and BRDF of ground surface at each pixel for accurate BRDF and topographic correction is unknown. Above all, reflectance of visible and infrared wavelengths saturate in dense vegetation. These problems affect accurate biomass and NPP estimation using optical images.

On the other hand, light detection and ranging (LiDAR) technology provides accurate canopy height information (Maltamo et al. 2014), which is one of the biophysical parameters. Although laser scanning emit laser pulses discretely, current laser scanner can emit more than 10 laser pulses per square meter to the ground from the air. Dense laser pulses provide pseudo wall-to-wall height information and can supply accurate canopy height of trees in a large area.

Laser scanning based on LiDAR from the air was introduced for forest measurements in the early 1980s, and a laser profiler revealed that tree canopy height was measurable from the air in a large area (Arp et al. 1982; Aldred and Bonner 1985). Airborne laser scanners emit laser pulses from the air to the ground and receive reflected pulses from objects on the ground. The geographical location of the ground object is determined from the time lag between the emission and receiving of the laser pulse (distance) and the direction from the scanner on airplane geographical

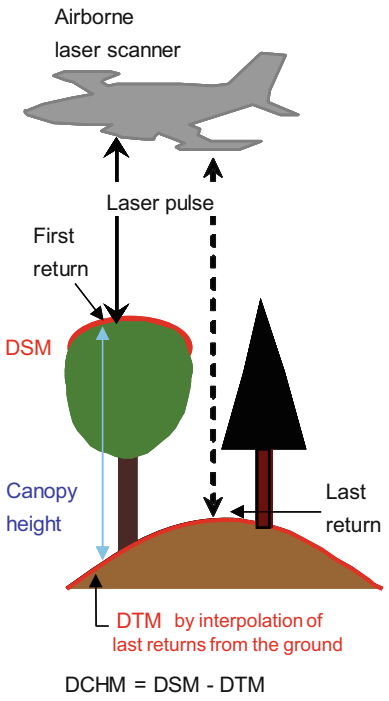

Fig. 4.1 Schematic view of laser scanning

location (Beraldin et al. 2010). Most pulses reflect at the canopy surface (first return) and few pulses reach to the ground (last return). Surface returns show surface elevation of objects and ground returns show the ground elevation. First returns are used to produce a digital surface model (DSM), and ground surface is estimated as a digital terrain model (DTM) using ground returns and numerical interpolation, such as triangulated irregular network (TIN, Maas 2010). The difference between DSM and DTM is the digital canopy height model (DCHM, Fig. 4.1). DCHM is accurate canopy information of not only height but also horizontal and vertical structure. Laser pulses also provide information on foliage.

Various research in this field has been carried out (Leeuwen and Nieuwenhuis 2010; Wulder et al. 2012). For example, stem volume or biomass estimation is the most popular and important research topic for forestry, forest ecology, and carbon circulation studies (Awaya and Takahashi 2017; Breidenbach et al. 2016; Takahashi et al. 2005a, 2010; Maltamo et al. 2004; Holmgren et al. 2003; Næsset 1997; Peng et al. 2019; Cao et al. 2014; Kankare et al. 2013; Mora et al. 2013; He et al. 2012; Rosette et al. 2012; Yao et al. 2011; Zhao et al. 2009; Foody et al. 2003; Lefsky et al. 1999a, b; Nelson et al. 1988).

Forest type or tree species classification using airborne LiDAR data is advantageous in precise canopy detection and species identification using the reflected laser pulse intensity or canopy attributes that are derived from the pulses (Hovi et al.

2016). Airborne LiDAR data provide canopy structure information such as vertical canopy cover (Korhonen et al. 2011) and vertical structure (Morsdorf et al. 2009). Forest gaps, which are open canopy areas in closed forest, can be detected (Zhang 2008) and monitored using time serial LiDAR data (Vepakomma et al. 2008, 2012; Araki and Awaya 2021). Gaps are important for undergrowth plants as they can get more sunlight; therefore, monitoring gaps and undergrowth plants give us prediction of tree regeneration. Scientists commonly use leaf area index (LAI) estimation. Optical images have been commonly used for LAI mapping (Melnikova et al. 2018; Biudes et al. 2014; Sprintsin et al. 2007; Knyazikhin et al. 1998; Spanner et al. 1990; Peterson et al. 1987) despite some difficulties with signal saturation, atmospheric effects, and topographic effects. Although atmospheric and topographic effects were able to be greatly reduced and seasonal and inter-annual LAI monitoring is possible, saturation was still a serious problem (Melnikova et al. 2018).

As for LAI prediction using LiDAR, its data provide better estimates compared to those by optical sensor data and even three-dimensional leaf distribution has been mapped (Sumnall et al. 2021; Almeida et al. 2019; Kamoskea et al. 2019; Hopkinson et al. 2013; Morsdorf et al. 2006). Thus, LiDAR data are useful not only for mapping of forest status but also for monitoring its changes, and the results are useful for forest management.

Among these applications, biomass estimation is the most important among carbon studies for understanding the capacity of a forest as a sink and pool of carbon. If airborne LiDAR data are captured twice within some years over the same forest, then tree growth such as height or biomass can be analyzed accurately over a wide area. The estimation provides growth potential information of trees in the coverage of LiDAR data.

Large-area forest inventory is a time-consuming task; however, biomass estimation using LiDAR point data has become popular for creating wall-to-wall inventories. LiDAR-based inventories are essential now in providing more accurate estimates of biophysical properties than conventional methods. Although airborne laser observation and data processing is costly, it provides forest resource information over large areas with wall-to-wall coverage. Indeed, the use of laser data for forest inventories supply promising results and improved accuracy (Næsset 2014). Various studies revealed the performance of airborne laser sensors for predicting forest variables, such as stem volume and above-ground biomass (AGB) of pine (Nelson et al. 1988), AGB of deciduous broadleaved and evergreen coniferous (Lefsky et al. 1999a, b) forests, and stem volume of evergreen coniferous forests, such as pine forests (Næsset 1997). The advanced LiDAR technology in pulse density and accurate positioning (Næsset 2014) brings accurate small-footprint laser data, which results in precise biomass mapping (Means et al. 2000; Holmgren et al. 2003).

Stem volume is proportional to the space between the canopy surface and the ground (hereafter, canopy space) (Tsuzuki et al. 2006). The average canopy height is determined by the canopy space divided by the stand area. Thus, the canopy space and average canopy height are identical and the average canopy height is useful for stem volume estimation. However, individual tree analysis has become popular for

variables, such as tree height (Kwak et al. 2007), AGB, and stem volume. Double-logarithmic relationships have been applied for single tree analysis between AGB or stem volume and variables from LiDAR data, including the average canopy height (Næsset and Økland 2002; Takahashi et al. 2005a, b; Kankare et al. 2013). Areal-based analysis produced much better results than individual tree-based analysis for stem volume and AGB (Kankare et al. 2013). Since most of numerous studies were stand-level studies, it is important to evaluate the causes of the estimate variation in the stand-level analysis prior to operational use (Breidenbach et al. 2016).

As described above, LiDAR data provide accurate biomass distribution maps, and if two biomass maps in a period are compared, the distribution of biomass changes become clear (Næsset and Gobakken 2005). As for LAI (leaf biomass), accurate estimation seems to be still difficult due to saturation of LAI against a number of return pulses. However, accurate woody biomass estimation is possible (Awaya and Takahashi 2017; Takahashi et al. 2010; Maltamo et al. 2004).

Therefore, woody biomass change can be mapped accurately in a large area using airborne LiDAR data (Næsset and Gobakken 2005). I herein introduce the usefulness of airborne LiDAR data for TDB and growth (TDB change) mapping in mountain forests in the middle of the main (Honshu) island of Japan.

4.2 The Study Site, Data and Method

The Japanese archipelago spreads between 20°N and 45°N between the subtropical and boreal zones. Therefore, various forest types (sub-tropical evergreen deciduous forest, temperate evergreen broadleaved forest, cool temperate deciduous broadleaved forest, and boreal evergreen coniferous forest) exist in the Japanese archipelago. About two-thirds of land in Japan is covered by forest; about 60% of the forest is naturally regenerated forest and the remainder is plantation forest containing coniferous trees such as Japanese cedar or sugi (*Cryptomeria japonica* D. Don), hinoki cypress (*Chamaecyparis obtusa* Sieb. et Zucc.), Japanese larch (*Lalix leptolepis* Gordon), Todo fir (*Abies sachalinensis* Masters), and Ezo spruce (*Picea jezoensis* Carr.).

Part of a small river basin was selected as the study area (36.146°N, 137.386°E). The study site was part of the Namai river basin, which is located near Takayama city in Gifu Prefecture. The elevation ranges between 800 and 1600 m above sea level (ASL) in the west and east, respectively, with a steep topography and an average slope angle of 30 degrees. The area is located in the cool temperate zone with natural deciduous broad-leaved forests and artificial coniferous forests, which are the most common forests in Honshu Island. According to local information, most of the river basin was completely logged about 60–70 years ago (after World War 2) and therefore the forests in the study site are relatively young. Plantation forests of evergreen conifers, including Japanese cedar and hinoki cypress, are dominant in the area below approximately 1000 m ASL. Planting of Japanese cedar seedlings was common in the 1950s and 1960s because Japanese cedar is a fast-growing species

Table 4.1 Summary of plot surveys between 2009 and 2013 (Awaya and Takahashi 2017)

Forest type	Stage	No of plots	Average DBH (cm)			Average tree Height (m)			TDB (Mg ha^{-1})		
Japanese cedar[a]	Young	4	1.1	–	9.4	1.8	–	5.8	2.6	–	86.1
	mature	8	22.6	–	41.2	18.8	–	29.1	325.7	–	467.1
Hinoki cypress[a]	Young-mature	21	14.6	–	34.3	9.6	–	21.4	110.4	–	444.9
Deciduous broadleaved		55	1.1	–	25.7	1.7	–	21.3	7.2	–	317.6

[a] Cedar, cypress and then cedar were planted in conifer plantations after World War II. Area of young cedar plantation is small

used for timber production including the rebuilding of destroyed houses after World War 2.

Hinoki cypress was introduced to Japan between the 1970s and 1990s because of its valuable commercial quality (Forestry Agency of Japan 2014). Japanese cedar has also been planted recently. Therefore the ages of Japanese cedar and hinoki cypress stands are clearly different in the study area. Natural deciduous broadleaved forests dominate in areas above 1000 m ASL, and planted Japanese larch forests exist in areas above 1200 m ASL. The most dominant deciduous broadleaved species in this region are deciduous oak (*Quercus mongoloca* var. grosseseratta Rehder et Wilson), Japanese white birch (*Betula platyphylla* var. japonica Hara), and Erman's birch (*Betula ermanii* Cham.).

Cherry spp. such as Japanese bird cherry (*Prunus grayana* Maxim.), maple spp. such as Redvein maple (*Acer rufinerve* Siebold & Zucc.), and Japanese umbrella tree (*Magnolia obovate* Thunb.) are common and vary with elevation and successional stages of stands. Japanese larch was planted around the 1950s for a short period, and the tree size is similar among larch stands.

Table 4.1 shows the summary of forest field data for biomass mapping. As shown in Fig. 4.2a, coniferous plantations (dark green) cover the lower part of slopes. Cedar has a rounder canopy than cypress (Fig. 4.2b) and it appears darker green than cypress in the areal photo, however, it was difficult to identify these species in the aerial photo (Fig. 4.2d). Deciduous broadleaved trees change in autumn to different leaf colors by species (Fig. 4.2c) and appear in dark brown in Fig. 4.2d.

There are two forest flux measurement sites within this study site (Fig. 4.2d): one at a deciduous broadleaved forest (TKY Takayama deciduous broadleaf forest site http://asiaflux.net/index.php?page_id=112) and the other at an evergreen coniferous forest (TKC Takayama evergreen coniferous forest site http://asiaflux.net/index.php?page_id=111). They have been operated since 1993 and 2005, respectively.

The main objective of the flux measurement sites is to measure atmospheric CO_2 flux, estimate its exchange between ecosystem and atmosphere, then understand the biological mechanisms. Numerous carbon flux (e.g. Saitoh et al. 2012), biological (e.g. Muraoka et al. 2012), and ecological (e.g. Ohtsuka 2012) studies have been executed in the flux measurement sites. Linking biological and ecological findings to

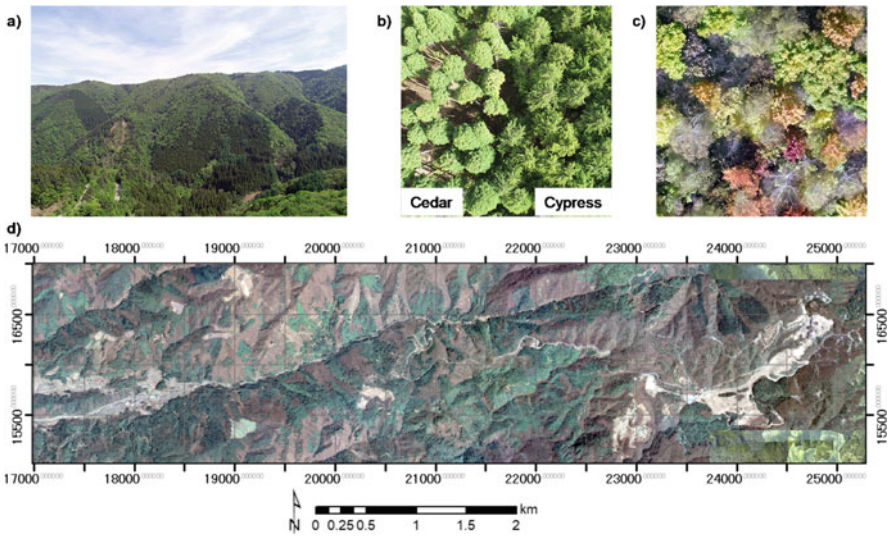

Fig. 4.2 Forest views in the study site and an aerial ortho-photo map. (**a**) A view of forest in this area. Topography is mountainous and steep. Dark green and brighter green parts are evergreen coniferous and deciduous broadleaved forest, respectively. UAV photos over (**b**) evergreen coniferous stands and (**c**) a deciduous broadleaved stand under autumnal coloring. (**d**) The orthophoto which were acquired in autumn, 2012 covers the entire study site. Deciduous trees had dropped leaves at the time of photo acquisition and appear in brown. The coordinate system of the orthophoto is Japan Plane Rectangular Coordinate System VII

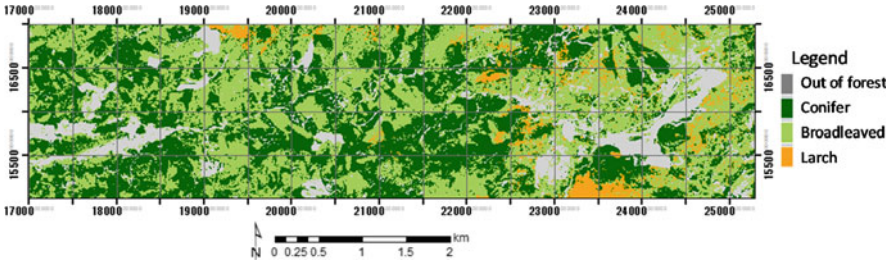

Fig. 4.3 Forest type map of the mapping area (Awaya and Takahashi 2017)

satellite remote sensing is one of primary objectives of the flux measurement sites (Muraoka et al. 2012).

4.2.1 Remote Sensing Data and Forest Type Map

Three airborne LiDAR datasets of the study area were obtained in October 2003, July 2005, and August 2011. The footprint sizes of the three LiDAR datasets were

between 0.2 and ca. 0.4 m, and the point densities were 0.7, 1.8, and 1.0 pulses m^{-2} for the 2003, 2005, and 2011 LiDAR data, respectively (Table 4.2).

LiADR data in 2003 was used to identify forest and non-forest area in the forest type classification with two QuickBird images in April 12, 2007 and May 23, 2007 (Fukuda et al. 2012) using a decision-tree classification procedure. A digital canopy height model (DCHM), comprising the difference between the digital surface model (DSM) and the digital terrain model (DTM), was produced using the LiDAR data of 2003 and used to separate forest and other land covers. Two QuickBird images were used for forest type classification to identify deciduous forest by phenological changes using the maximum likelihood classifier, and separated from evergreen coniferous forest. The forest-type map (Fig. 4.3) was used as a reference to check forest type distribution, and for selection of biomass prediction models by the forest type at each pixel.

Forests were classified into three types in the map: evergreen coniferous forests (Japanese cedar and hinoki cypress), deciduous broadleaved forests, and larch forests. Coniferous plantations seemed prevalent in areas where there was easy access for people (Fig. 4.3). A prefectural road extending from west to east is the main road in the study area. The road appeared in black on DCHM (Fig. 4.4b). Some forest roads extend from this prefecture road to forest plantations. Elevation was higher in the eastern part where deciduous broadleaved forest was common. The acreages of evergreen coniferous forest and deciduous broadleaved forest are almost the same in this area.

The Namai river flows from a mountain peak in the north-east (top of Fig. 4.4a) and then flows alongside flat land. Other parts are mountainous and steep. Tall trees exist mostly in the west along the Namai river, and trees are small in the east, as described previously (Fig. 4.4b).

4.2.2 Biomass Estimation Model

It was pointed out that there was a linear relationship between average canopy height and stem volume or biomass (Tsuzuki et al. 2006). Average canopy height and various canopy parameters are computed from LiADR point cloud data. The LiDAR parameter with highest correlation against TDB was different according to forest type (Awaya and Takahashi 2017); however, there were some parameters that had significant correlation with TDB.

TDB prediction models for evergreen coniferous and deciduous broadleaved forests were produced by a linear regression analysis using parameters with the highest correlation coefficients with TDB among LiDAR parameters. Average canopy height and a half height of canopies were selected as the independent variables for evergreen coniferous and broadleaved deciduous forest, respectively, as shown in Fig. 4.5 (Awaya and Takahashi 2017). The model for deciduous broadleaved forests was used for larch forests.

Evergreen coniferous forest:

Table 4.2 Summary of LiDAR observations

Observation date	Laser scanner	Beam divergence (mrad)	Wavelength (nm)	Flight altitude above ground (m)	Footprint size (m)	FOV (°)	Beam density (pulse m^{-2})	Usage
Oct., 2003	RAMS (EnerQuest, USA)	0.33	1064	2000 (Entire Gifu Prefecture)	–	±22	0.7	Classification
July 25, 2005	ALTM 2050DC (Teledyne Optech, Canada)	0.19	1064	1200	0.24	±22	1.8	Biomass estimation
Aug. 28, 2011	VQ-580 (RIEGL, Horn, Austria)	0.50	1550	600	0.30	±30	1.0	Biomass estimation

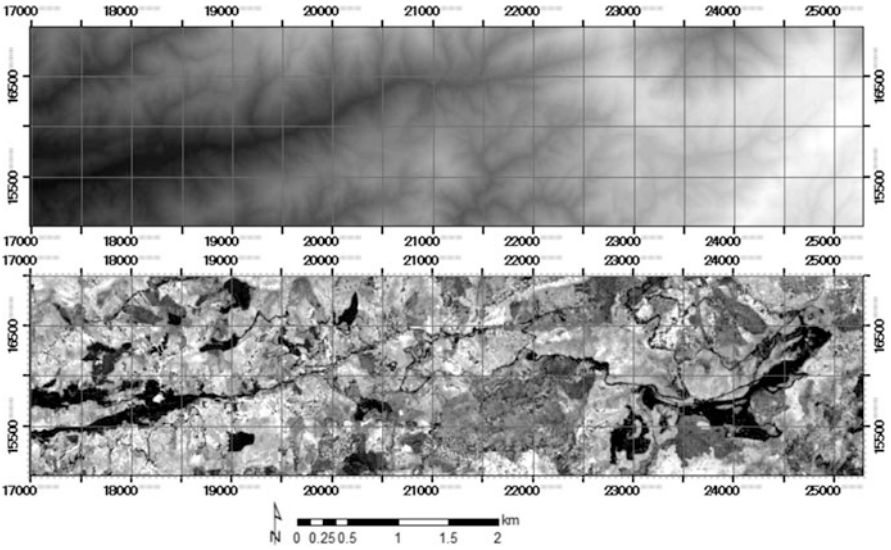

Fig. 4.4 Airborne LiDAR data over the study site. (**a**) A digital surface model (DSM): objects with higher elevation appear brighter. Elevation is lower in the western part which is connecting to the Takayama city area. (**b**) A digital canopy height model (DCHM), which was obtained in August, 2011: black areas are open areas such as roads, crop fields, open recreation areas, and ski slopes

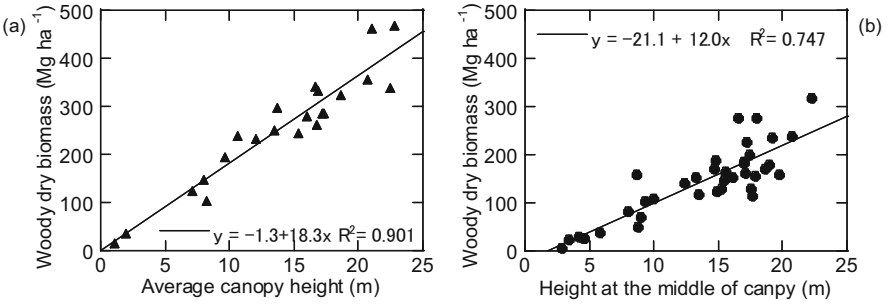

Fig. 4.5 Relationship canopy parameters, which were computed using DCHM in 2011 and field-measured the total (above and below) woody dry biomass. (**a**) Evergreen coniferous forest, and (**b**) deciduous broadleaved forest

$$\mathrm{TDB} = 18.3 \times \mathrm{AHavr} - 1.3 \tag{4.1}$$

Deciduous broadleaved forest:

$$\mathrm{TDB} = 12.0 \times \mathrm{Hd5} - 21.1 \tag{4.2}$$

There is a strong correlation between the independent variables and TDB for the two forest types. The validation results showed the usefulness and weakness of DCHM

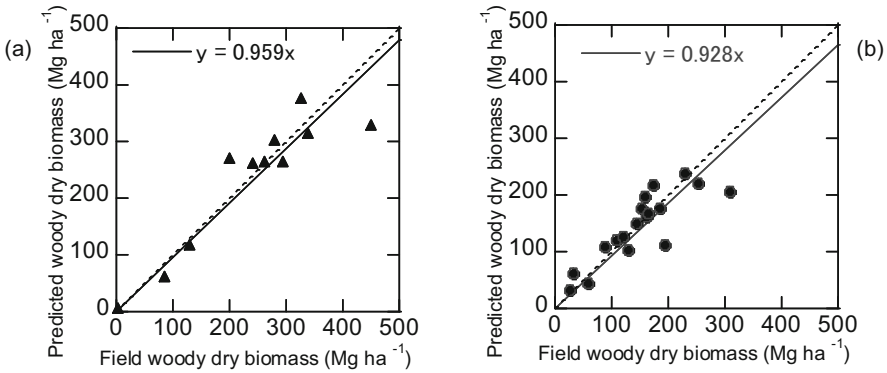

Fig. 4.6 Validation results of TDB prediction based on the comparison of predicted and field TDB. Models (**a**) for evergreen coniferous forests, and (**b**) for deciduous broadleaved forests (Awaya and Takahashi 2017)

derived variables. Predicted TDB tended to be slightly underestimated as the regression lines, with slopes of 0.959 and 0.928 between field measurements (X-axis) and the predictions (Y-axis) in Fig. 4.5. The size variation would be a function of age and, thus, canopy height. Therefore, LiDAR height variables probably correlated with variation in biomass among stands. Reducing standard error is the greatest task in improving the accuracy of TDB estimates, and adding the second height variable may be effective.

The models for coniferous forests might underestimate the Japanese cedar field TDB and overestimate the hinoki cypress field TDB. Japanese cedar trees had a multilayer structure because of intraspecies competition under unthinned conditions. The overstory canopies covered understory trees that were invisible from the air. Therefore the estimated TDB was relatively low, because the understory was not evaluated in the overall estimation using the DCHMs and prediction model.

On the other hand, hinoki cypress stands had an uniform one-layer canopy and relatively low TDB in this area, resulting in an overestimate using the DCHMs and prediction model. Thus, canopy structure influences the biomass estimates (Rosette et al. 2012). The standard errors (SEs) for TDB validation (Fig. 4.6) were 32.3 and 35.8 Mg ha^{-1} for evergreen coniferous forest and deciduous broadleaved forest, respectively. Estimates were sensitive to the tree density or canopy structure. Dense stands tended to result in underestimations with high SEs.

4.3 Biomass Distribution

TDB maps were produced using raster LiDAR parameter files, the forest type map (Fig. 4.3), and selected models (Fig. 4.5). A frequency histogram of the 2011 TDB map (not shown) had a symmetrical frequency distribution peaking at around

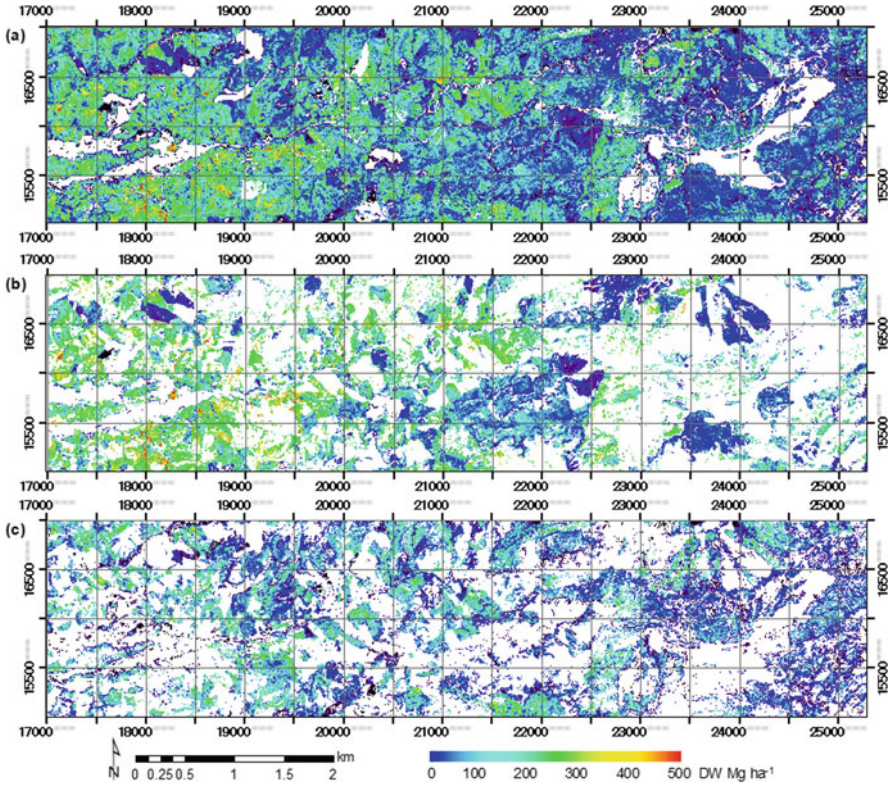

Fig. 4.7 Distribution of TDB 2005 predicted using Eqs. (4.1) and (4.2). (**a**) All forest, (**b**) evergreen coniferous forest, and (**c**) deciduous broadleaved forest

230 Mg ha^{-1} (Awaya and Takahashi 2017), while the average was 239.4 Mg ha^{-1}. There was no clear deviation of biomass frequency when all forests were considered.

TDB maps show forest status regarding woody biomass distribution well. TDB was greater in the western half than that in the eastern half of the study area, both in 2005 (Fig. 4.7a) and 2011 (Fig. 4.8a). TDB was especially great around the open area in the west where local farmers' houses existed. As described previously, Japanese cedar was planted after the World War 2 before the planting of hinoki cypress, therefore it had the highest TDB in the western part in Figs. 4.7a and 4.8a.

A small village was located at the west and forest farmers planted evergreen coniferous trees in their surroundings. Deciduous broadleaved trees were used as fuel wood until about 1960 before the energy revolution, and most broadleaved forest seemed to have been left undisturbed and thus regenerated naturally. Hence, areas with high TDB in the west mainly included mature Japanese cedar forests. On the other hand, there was no residential area in the eastern two-thirds, and planting trees started later than the western area near the village. As a result, broadleaved and

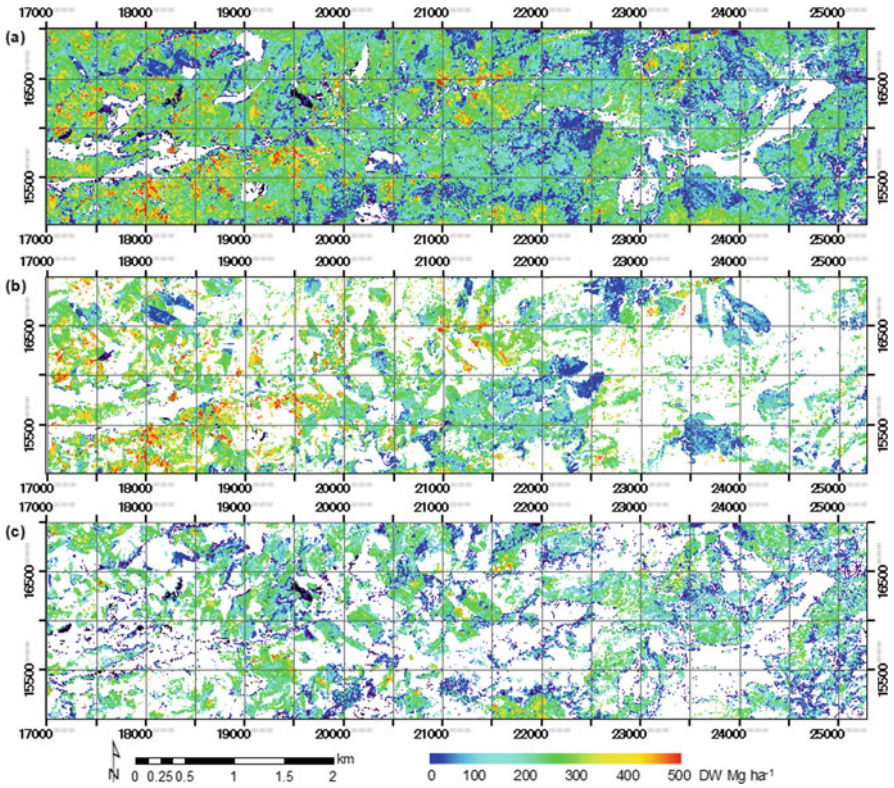

Fig. 4.8 Distribution of TDB 2011 predicted using Eqs. (4.2) and (4.8). (**a**) All forest, (**b**) evergreen coniferous forest, and (**c**) deciduous broadleaved forest (Awaya and Takahashi 2017)

young coniferous forests with small TDB dominated in the eastern two-thirds of the mapping area.

TDB of evergreen coniferous forest exceeded 300 Mg ha^{-1} in 2005 (Fig. 4.7b) and became greater in 2011 (Fig. 4.8b) in the west. On the other hand, TDB of evergreen coniferous forest was mostly less than 200 Mg ha^{-1} with the same level of deciduous broadleaved forest in the eastern one-third in 2005 (Fig. 4.7c), and the trend was the same in 2011 (Fig. 4.8c), although TDB increased up to about 300 Mg ha^{-1}. Thus harvesting and planting history influenced on the biomass distribution in the study site and the TDB maps shows the forestry history activity indirectly. Thus, historical human activity reflected the distribution of forest types and biomass in this area.

4.4 Interannual Biomass Change

Logging was rare between 2005 and 2011 because stands were in the pre-mature stage and mostly less than 50 years old, which is the standard time to harvest cedar and cypress trees in this area. Therefore biomass increased everywhere (Fig. 4.9). On the other hand, biomass decreased in only 2.6% of the forest area. The area in which biomass decreased more than 100 Mg ha^{-1} was only 0.8% of the forest where trees would be logged. The TDB change map shows that TDB increased greater in evergreen coniferous forest than in deciduous broadleaved forest. Japanese cedar grows fast among tree species in Japan so this would be the greatest reason of this difference.

The annual TDB growth of the Japanese cedar almost reaches greatest in about 50 years old, and the stand age of most cedar forests was about 40 to 50 years in the study site. These are probably the reasons of greater TDB increase in the coniferous forests than broadleaved forests, and TDB increase was more than 5 Mg ha^{-1} year^{-1} in large parts of the coniferous forests. On the other hand, TDB increased mostly

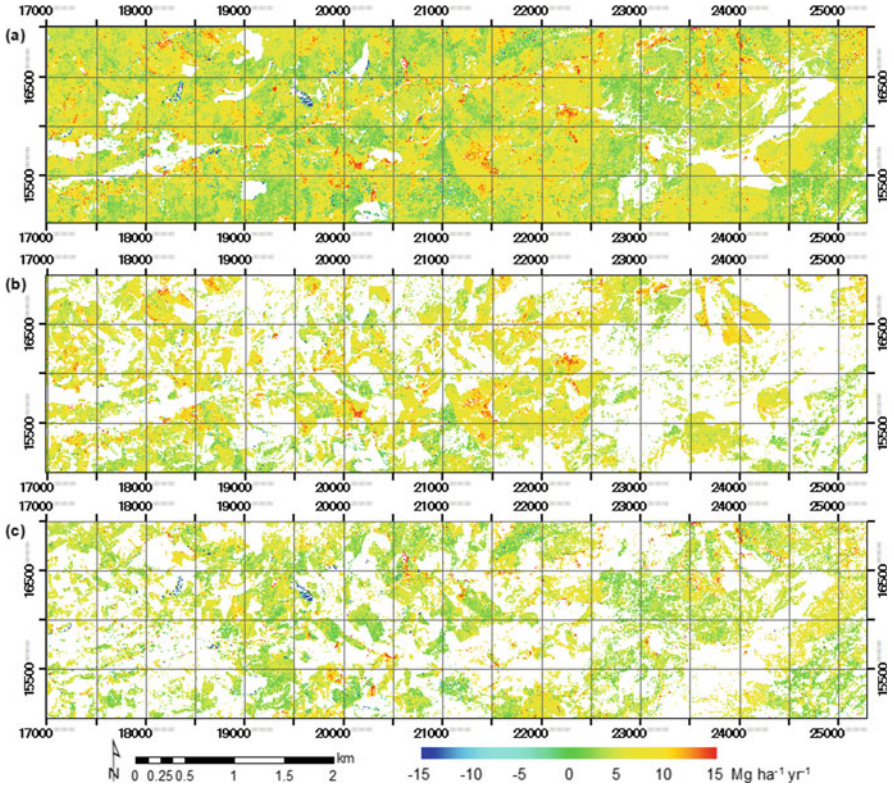

Fig. 4.9 Secular TDB change between 2005 and 2011. (**a**) All forest, (**b**) evergreen coniferous forest, and (**c**) deciduous broadleaved forest

around 5 Mg ha^{-1} year^{-1}, and the area with increase less than 5 Mg ha^{-1} year^{-1} covered about a half of the map (Fig. 4.9).

Table 4.3 shows TDB in 2005 and 2011 along with its change. The average TDB of evergreen coniferous forest was about 1.4 times greater than that of deciduous broadleaved forest, both in 2005 and 2011. Annual TDB changes were 6.6 and 3.6 Mg ha^{-1} year^{-1} for these forest types, respectively, and 5.0 Mg ha^{-1} year^{-1} for all forest.

Thus evergreen coniferous forest had greater TBD and growth rate than deciduous broadleaved forest. Since the forest age is probably similar due to a common harvesting and planting history of trees for the two forest types in this area, the difference would be caused by difference rates of growth between the tree species rather than different stand ages between the two forest types. Since the coverage area of these forest types was similar in this area, TDB of evergreen coniferous forests was about 1.3 times that of broadleaved forests in 2005 and 2011; the ratio was almost same as the ratio of average TDB. Total TDB change or woody biomass growth was 7213 MgDW ha^{-1} year^{-1} or 3607 MgC ha^{-1} year^{-1}, including larch.

Our results showed TDB distribution including above ground and underground woody parts of trees. Average annual change of TDB (growth) of deciduous broadleaved forest was about 3.6 MgDW ha^{-1} over the broadleaved forest and 2.38 MgDW ha^{-1} in TKY. An average annual woody biomass growth of 2.56 MgDW ha^{-1} was recorded between 1999 and 2009 in TKY (Ohtsuka 2012), which was quite close to the prediction by TDB difference. Ohtsuka (2012) also reported that the average annual leaf biomass was 3.66 MgDW ha^{-1}. Therefore the sum of woody biomass growth and leaf biomass, which is NPP, would be nearly twice of our TDB growth estimation in deciduous broadleaved forests.

4.5 Conclusions

As airborne laser scanners provide the most accurate canopy height information in a large area, researchers are keen to validate its accuracy for various forest applications using predicted biomass (stem, woody part, leaf) canopy structure. This article introduced an application of TDB and growth mapping regarding usages of airborne LiDAR data in forestry and carbon circulation.

High coefficients of determination appeared in the TDB prediction models of coniferous forest as well as in the broadleaved forest using canopy height parameters which were computed using airborne LiDAR data in 2011. The TDB prediction models were suitable for TDB mapping in a forested area comprising part of the Namai river basin.

Although field plot surveys provide biomass or carbon amount information, spatial distribution mapping is difficult due to hardiness of numerous plot surveys. The Forestry Agency of Japan has executed national forest inventory for more than 20 years; however, plots are located at 4 km lattice points. Thus spatial distribution of biomass cannot be mapped by plot surveys. Above all, repeating large scale

Table 4.3 Summary of TDB and its change by each forest type

Forest type	Area (ha)	Rate per whole area (%)	Rate per forest (%)	Average TDB (Mg ha^{-1})			Total TDB (Mg)			Rate of TDB (%)		
				2005	2011	Change per year	2005	2011	Change per year	2005	2011	Change
Evergreen Conif.	664.4	40.0	46.1	253.0	292.5	6.6	168,063	194,353	4384	53.9	54.7	60.5
Deciduous DRD	708.6	42.7	49.2	184.4	205.9	3.6	130,695	145,888	2559	41.9	41.1	35.3
Larch	68.4	4.1	4.7	193.9	220.1	4.4	13,261	15,059	299	4.3	4.2	4.1
Sub total or mean	1441.4	86.8	100.0	216.5	246.5	5.0	312,019	355,300	7242	100.0	100.0	100.0
None forest	218.6	13.2										
Total	1660.0	100.0										

precise survey is costly. Airborne laser observations are also costly; however, point clouds height data provide accurate biomass maps and are stored for further analysis.

As shown in this article, biomass (TDB) maps using repetitive observation data resulted in a biomass change (TDB growth or NPP) map which showed carbon fixation by forest plants. Unlike carbon flux measurements, it is impossible to map carbon fixation by forested lands (Net Ecosystem Production, NEP) using airborne LiDAR alone. If soil respiration is estimated using remote sensing data (including climate), carbon fixation can be mapped and would be advantageous. However, a comparison of NPP between LiDAR estimates and field survey in TKY showed a close agreement. Although NEP mapping using LiDAR data is difficult, NPP mapping is quite accurate and LiDAR remote sensing can provide spatial distribution of biomass growth or carbon fixation by trees.

Our results are transferrable to forests of the same species with a similar structure. Unfortunately, our results will not be universal among various forests, however, as pointed out by other studies (Næsset 2014; Rosette et al. 2012). Forest structure varies greatly and is impacted, for example, by planting rates or thinning practices. Estimation errors would be great after thinning which changes stand structure. This can result in changes in the relationship between biomass and LiDAR variables (Rosette et al. 2012). The difference in stand structure, including canopy height and variation, is especially influenced by thinning and must, therefore, have great influence on TDB prediction which was derived using canopy height parameters.

It was necessary to reduce effects by stand density and slope angle, which reduced the accuracy of DCHM using probably very dense point cloud data. LiDAR technology has advanced greatly and precise forest biomass mapping is promising using future airborne LiDAR data.

Acknowledgments This article was the result of a research project "Development of an accuracy assessment method for scaling results of carbon balance using a process based model" supported by JSPS KAKENHI (grant number 22248017, Grant-in-Aid for Scientific Research A). The 2003 LiDAR data and three aerial orthophotos were provided by the Gifu Prefectural Government. The author appreciates the work of Emeritus Professor Tsuyoshi Akiyama who contributed to the research by establishing research facilities in Takayama, such as image processing software, the QuickBird images, and the 2005 LiDAR data. The author greatly appreciates the valuable advice from Dr. Tomoaki Takahashi (Forestry and Forest Products Research Institute). The author also appreciates the field survey support from Mr. Kenji Kurumado (Takayama Research Center of Gifu University), Naoko Fukuda, and Hiroto Kawai (former Awaya Laboratory staff), and Siqinbilige Wang, Nabuti Alatan, and Weilisi (former Awaya Laboratory students).

References

Aldred AH, Bonner GM (1985) Application of airborne lasers to forest surveys (Inst. Information report PI-X-51); Petawawa National Forestry, Petawawa, pp 1–62

Almeida DRA, Stark SC, Shao G, Schietti J, Nelson BW, Bruce W, Silva CA, Gorgens EB, Valbuena R, Papa DA, Brancalion PHS (2019) Optimizing the remote detection of tropical

rainforest structure with airborne lidar: leaf area profile sensitivity to pulse density and spatial sampling. Remote Sens 11(1):92. https://doi.org/10.3390/rs11010092

Araki K, Awaya Y (2021) Analysis and prediction of gap dynamics in a secondary deciduous broadleaf Forest of Central Japan using airborne multi-LiDAR observations. Remote Sens 13(100). https://doi.org/10.3390/rs13010100

Arp H, Griesbach JC, Burns JP (1982) Mapping in tropical forests; A new approach using the laser APR. PE&RS 48:91–100

Awaya Y, Takahashi T (2017) Evaluating the differences in modeling biophysical attributes between deciduous broadleaved and evergreen conifer forests using low-density small-footprint LiDAR data. Remote Sens 9(572). https://doi.org/10.3390/rs9060572

Awaya Y, Kodani E, Tanaka K, Liu J, Zhuang D, Meng Y (2004) Estimation of the global net primary productivity using NOAA images and meteorological data: changes between 1988 and 1993. Int J Remote Sensing 25(9):1597–1613

Beraldin J, Blais F, Lohr U (2010) Laser scanning technology. In: Vosselman G, Mass H (eds) Airborne and terrestrial laser scanning. Whittles Publishing, Scotland, pp 19–30

Biudes MS, Machado NG, Danelichen VH, Souza MC, Vourlitis GL, Nogueira JDS (2014) Ground and remote sensing-based measurements of leaf area index in a transitional forest and seasonal flooded forest in Brazil. Int J Biometeorol 58:1181–1193

Breidenbach J, McRoberts RE, Astrupa R (2016) Empirical coverage of model-based variance estimators for remote sensing assisted estimation of stand-level timber volume. Remote Sens Environ 173:274–281

Cao L, Coops NC, Hermosilla T, Innes J, Dai J, She G (2014) Using small-footprint discrete and full-waveform airborne lidar metrics to estimate total biomass and biomass components in subtropical forests. Remote Sens 6:7110–7135

Food and Agriculture Organization of the United Nations (FAO) (2016) Global forest resources assessment 2015 how are the world's forests changing? 2nd edn. FAO, Rome, pp 1–44

Foody GM, Boydb DS, Cutlerc MEJ (2003) Predictive relations of tropical forest biomass from Landsat TM data and their transferability between regions. Remote Sens Environ 85:463–474

Forestry Agency of Japan (2014) Annual report on Forest and forestry in Japan fiscal year 2013. Forestry Agency of Japan, Tokyo, p 223. (In Japanese with English Summary)

Franklin SE (2001) Remote sensing for sustainable forest management. Lewis Publishers, CRC Press, Florida, 407 pp

Fukuda N, Awaya Y, Kojima T (2012) Classification of forest vegetation types using LiDAR data and Quickbird images – case study of the Daihachiga river basin in Takayama city. J JASS 28: 115–122. (In Japanese with English Summary)

He QS, Cao CX, Chen EX, Sun GQ, Ling FL, Pang Y, Zhang H, Ni WJ, Xu M, Li ZY (2012) Forest stand biomass estimation using ALOS PALSAR data based on LiDAR-derived prior knowledge in the Qilian Mountain, western China. Int J Remote Sens 33:710–729

Holmgren J, Nilsson M, Olsson H (2003) Estimation of tree height and stem volume on plots using airborne laser scanning. For Sci 49:419–428

Hopkinson C, Lovell J, Chasmer L, Jupp D, Kljun N, van Gorsel E (2013) Integrating terrestrial and airborne lidar to calibrate a 3D canopy model of effective leaf area index. Remote Sens Environ 136:301–314

Houghton JH, Ding Y, Grigss DJ, Noguer M, van der Linden PJ, Xiaosu D (eds) (2001) Climate change 2001: the scientific basis. Cambridge University Press, Cambridge, pp 99–237

Hovi A, Korhonen L, Vauhkonen J, Korpela I (2016) LiDAR waveform features for tree species classification and their sensitivity to tree- and acquisition related parameters. Remote Sens Environ 173:224–237

Kamoskea AG, Dahlina KM, Starkc SC, Shawn P, Serbind SP (2019) Leaf area density from airborne LiDAR: comparing sensors and resolutions in a temperate broadleaf forest ecosystem. For Ecol Manag 433:364–375

Kankare V, Vastaranta M, Holopainen M, Räty M, Yu X, Hyyppä J, Hyyppä H, Alho P, Viitala R (2013) Retrieval of forest aboveground biomass and stem volume with airborne scanning LiDAR. Remote Sens 5:2257–2274

Knyazikhin Y, Martonchik J, Diner D, Myneni R, Verstraete M, Pinty B, Gobron N (1998) Estimation of vegetation canopy leaf area index and fraction of absorbed photosynthetically active radiation from atmosphere-corrected MISR data. J Geophys Res Atmos 103:32239–32256

Korhonen L, Korpela I, Heiskanen J, Maltamo M (2011) Airborne discrete-return LIDAR data in the estimation of vertical canopy cover, angular canopy closure and leaf area index. Remote Sens Environ 115:1065–1080

Kwak D, Lee W, Lee J, Biging GS, Gong P (2007) Detection of individual trees and estimation of tree height using LiDAR data. J For Res 12:425–434

Leeuwen M, Nieuwenhuis M (2010) Retrieval of forest structural parameters using LiDAR remote sensing. Eur J Forest Res 129:749–770

Lefsky MA, Harding D, Cohen WB, Parker G, Shugart HH (1999a) Surface lidar remote sensing of basal area and biomass in deciduous forests of eastern Maryland, USA. Remote Sens Environ 67:83–98

Lefsky MA, Cohen WB, Acker SA, Parker GC, Spies TA, Harding D (1999b) Lidar remote sensing of the canopy structure and biophysical properties of Douglas-fir western hemlock forests. Remote Sens Environ 70:339–361

Maas H (2010) Forestry applications. In: Vosselman G, Mass H (eds) Airborne and terrestrial laser scanning. Whittles, Scotland, pp 213–235

Maltamo K, Eerikäinenn J, Pitkänen J, Hyyppä M (2004) Vehmas estimation of timber volume and stem density based on scanning laser altimetry and expected tree size distribution functions. Remote Sens Environ 90:319–330

Maltamo M, Næsset E, Vauhkonen J (eds) (2014) Forestry applications of airborne laser scanning. Springer, Dordrecht, 464 pp

Means JE, Acker SA, Fitt BJ, Renslow M, Emerson L, Hendrix CJ (2000) Predicting forest stand characteristics with airborne scanning lidar. PE&RS 66:1367–1371

Melnikova I, Awaya Y, Saitoh TM, Muraoka H, Sasai T (2018) Estimation of leaf area index in a mountain Forest of Central Japan with a 30-m spatial resolution based on Landsat operational land imager imagery: an application of a simple model for seasonal monitoring. Remote Sens 10:179. https://doi.org/10.3390/rs10020179

Mora B, Wulder MA, White JC, Hobart G (2013) Modeling stand height, volume, and biomass from very high spatial resolution satellite imagery and samples of airborne LiDAR. Remote Sens 5:2308–2326

Morsdorf F, Kötz B, Meier E, Itten KI, Allgöwer B (2006) Estimation of LAI and fractional cover from small footprint airborne laser scanning data based on gap fraction. Remote Sens Environ 104(1):50–61

Morsdorf F, Nichol C, Malthus T, Woodhouse IH (2009) Assessing forest structural and physiological information content of multi-spectral LiDAR waveforms by radiative transfer modelling. Remote Sens Environ 113:2152–2163

Muraoka H, Noda HM, Saitoh TM, Nagai S, Nasahara KN (2012) Long-term and regional scale observation of forest canopy photosynthesis by linking plant ecophysiology and satellite remote sensing. BSJ-Review 3, 16 pp

Næsset E (1997) Estimating timber volume of forest stands using airborne laser scanner data. Remote Sens Environ 61:246–253

Næsset E (2014) Area-based inventory in Norway-from innovation to an operational reality. In: Maltamo M, Næsset E, Vauhkonen J (eds) Forestry applications of airborne laser scanning, vol 27. Springer, Dordrecht, pp 215–240

Næsset E, Gobakken T (2005) Estimating forest growth using canopy metrics derived from airborne laser scanner data. Remote Sens Environ 96:453–465

Næsset E, Økland T (2002) Estimating tree height and tree crown properties using airborne scanning laser in a boreal nature reserve. Remote Sens Environ 79:105–115

Nelson R, Krabill W, Tonelli J (1988) Estimating forest biomass and volume using airborne laser data. Remote Sens Environ 24:247–267

Ohtsuka T (2012) Carbon cycling at Takayama Forest: results from intensive studies in the last decade, and further studies for a next decade. Jpn J Ecol 62:31–44

Peng D, Zhang H, Liu L, Huang W, Huete AR, Zhang X, Wang F, Yu L, Xie Q, Wang C, Luo S, Li C, Zhang B (2019) Estimating the aboveground biomass for planted forests based on stand age and environmental variables. Remote Sens 11(2270). https://doi.org/10.3390/rs11192270

Peterson DL, Spanner MA, Running SW, Teuber KB (1987) Relationship of thematic mapper simulator data to leaf area index of temperate coniferous forests. Remote Sens Environ 22:323–341

Potter CS, Randerson JT, Field CB, Matson PA, Vitousek PM, Mooney HA, Klooster SA (1993) Terrestrial ecosystem production: a process model based on global satellite and surface data. Glob Biogeochem Cycles 7:811–841

Rosette J, Suárez J, Nelson R, Los S, Cook B, North P (2012) Lidar remote sensing for biomass assessment, in remote sensing of biomass—principles and applications. In: Fatoyinbo T (ed) InTech, Rijeka, pp 3–26

Saitoh TM, Nagai S, Yoshino J, Muraoka H, Saigusa N, Tamagawa I (2012) Functional consequences of differences in canopy phenology for the carbon budgets of two cool-temperate Forest types: simulations using the NCAR/LSM model and validation using tower flux and biometric data. Eurasian J Forest Res 15(1):19–30

Spanner MA, Pierce LL, Peterson DL, Running SW (1990) Remote sensing of temperate coniferous forest leaf area index. The influence of canopy closure, understory vegetation and background reflectance. Int J Remote Sens 11:95–111

Sprintsin M, Karnieli A, Berliner P, Rotenberg E, Yakir D, Cohen S (2007) The effect of spatial resolution on the accuracy of leaf area index estimation for a forest planted in the desert transition zone. Remote Sens Environ 109:416–428

Sumnall MJ, Trlica A, Carter DR, Cook RL, Schulte ML, Campoe OC, Rubilar RA, Wynne RH, Thomas VA (2021) Estimating the overstory and understory vertical extents and their leaf area index in intensively managed loblolly pine (Pinus taeda L.) plantations using airborne laser scanning. Remote Sens Environ 112250. https://doi.org/10.1016/j.rse.2020.112250

Takahashi T, Yamamoto K, Senda Y, Tsuzuku M (2005a) Predicting individual stem volumes of sugi (Cryptomeria japonica D. Don) plantations in mountainous areas using small-footprint airborne LiDAR. J For Res 10:305–312

Takahashi T, Yamamoto K, Senda Y, Tsuzuku M (2005b) Estimating individual tree heights of sugi (Cryptomeria japonica D. Don) plantations in mountainous areas using small-footprint airborne LiDAR. J For Res 10:135–142

Takahashi T, Awaya Y, Hirata Y, Furuya N, Sakai T, Sakai A (2010) Stand volume estimation by combining low laser-sampling density LiDAR data with QuickBird panchromatic imagery in closed-canopy Japanese cedar (Cryptomeria japonica) plantations. Int J Remote Sensing 31(5): 1281–1301

Tsuzuki H, Kusakabe T, Sueda T (2006) Long-range estimation of standing timber stock in western boreal forest of Canada using airborne laser altimetry. J Jpn For Soc 88:103–113. (In Japanese with English Summary)

Vepakomma U, St-Onge B, Kneeshaw D (2008) Spatially explicit characterization of boreal forest gap dynamics using multi-temporal lidar data. Remote Sens Environ 112:2326–2340

Vepakomma U, Kneeshaw D, Fortin MJ (2012) Spatial contiguity and continuity of canopy gaps in mixed wood boreal forests: persistence, expansion, shrinkage and displacement. J Ecol 100: 1257–1268

Wulder MA, White JC, Nelson RF, Næsset E, Ørka OH, Coops NC, Hilker T, Bater CW, Gobakken T (2012) Lidar sampling for large-area forest characterization: a review. Remote Sens Environ 121:196–209

Yao T, Yang X, Zhao F, Wang Z, Zhang Q, Jupp D, Lovell J, Culvenor D, Newnham G, Ni-Meister W (2011) Measuring forest structure and biomass in New England forest stands using echidna ground-based lidar. Remote Sens Environ 115:2965–2974

Zhang K (2008) Identification of gaps in mangrove forests with airborne LIDAR. Remote Sens Environ 112:2309–2325

Zhao K, Popescu S, Nelson R (2009) Lidar remote sensing of forest biomass: a scale-invariant estimation approach using airborne lasers. Remote Sens Environ 113:182–196